Synthesis of ZnO/Bi_2O_3 and $SnO_2/Bi_2O_3/Bi_2O_4$ mixed oxides and their photocatalytic activity

Maryam Movahedi[a],*, Akram Hosseinian[b], Nasrin Nazempour[a], Mohadeseh Rahimi[a], Hossein Salavati[a]

[a]Department of Chemistry, Payame Noor University, P.O. BOX 19395-3697, Tehran, Iran

[b]Department of Engineering Science, University College of Engineering, University of Tehran, P.O. BOX 11365-4563, Tehran, Islamic Republic of Iran

Abstract

In the present work, ZnO/Bi_2O_3, $SnO_2/Bi_2O_3/Bi_2O_4$ mixed oxide, Bi_2O_3 rod-like and SnO_2 nanoparticle have been synthesized. The obtained samples were characterized by field emission scanning electron microscopy (FE-SEM) and X-ray diffraction (XRD). The optical properties of samples were evaluated by UV-Vis spectrophotometer. The photocatalytic activity of samples was evaluated by decolorization of methylene blue (M.B.) solution. The Present work indicates the improving or hampering effect of Bi_2O_3 on the photocatalytic activity of ZnO/Bi_2O_3. The results show that the photocatalytic performance of ZnO/Bi_2O_3 which is higher than that of Bi_2O_3, SnO_2, and $SnO_2/Bi_2O_3/Bi_2O_4$ is related to the presence of the zinc oxide semiconductor. Furthermore, results indicated that the photoactivity of the SnO_2/Bi_2O_3 system was not improved. The present work affirms the importanat position of energy levels and also the separation of photogenerated electron/hole pairs on the efficient photocatalytic performance.

Keywords: Mixed oxide; Photocatalyst; Semiconductor; ZnO/Bi_2O_3; $SnO_2/Bi_2O_3/Bi_2O_4$.

*Corresponding author: Maryam Movahedi
Tel: +98 (31) 33522055, Fax: +98 (31) 33521700
E-mail: m.movahedi@pnu.ac.ir

Introduction

Removal of organic pollutants in wastewater is an important measure of environmental protection. Advanced oxidation processes (AOPs) provide a promising technique for the treatment of textile industry wastewater. The photocatalytic process, based on UV-Vis irradiated semiconductor, represents one of AOPs that provide an interesting route to the destruction of many organic substances of CO_2, H_2O, and corresponding mineral acids. When the semiconductor is illuminated by a photon of energy equal or higher than the band gap energy, electrons in the conduction band (e^-_{CB}) and holes in the valence band (h^+_{VB}) are produced. These charge carriers can recombine, or the holes can be scavenged by oxidizing species (for example, H_2O, OH^-), and electrons can be consumed by reducible species (for example, O_2) in the solution. The hydroxyl radical ($^\bullet OH$) is a highly reactive oxidizing reagent and can decompose most organic contaminants. So far, various kinds of compound materials, such as metal oxide and nanocomposites have been widely used as a photocatalyst [1-10]. In the present study, $SnO_2/Bi_2O_3/Bi_2O_4$, ZnO/Bi_2O_3 mixed oxide, Bi_2O_3 rod-like and SnO_2 nanoparticle have been synthesized. The photocatalytic activity of the prepared samples was evaluated by the decolorization of methylene blue (M.B.) solution under the UV-Vis irradiation.

Experimental

General

All the analytical chemicals were purchased from Merck and used without further purification. The detailed synthesis procedure is as follows:

Synthesis procedure for Bi_2O_3 preparation

The synthesis of Bi_2O_3 used for this study fundamentally followed a method reported previously by Wang *et al.* [11]. First, 200 mL of (0.2 M) NaOH solution was prepared (Solution I). Second, 2 g of $Bi(NO_3)_3.5H_2O$ was dissolved in 20 mL of the 1 M nitric acid solution (Solution II). Then, the solution (II) was added drop wise into the solution (I) under constant stirring. After stirring the mixture for 30 min at 80 ℃, the product was separated by decantation, washed with double distilled water several times and dried at 60 ℃. Then, heat treatment of the product was carried out at 600 °C for 1 h.

Synthesis procedure for ZnO/Bi_2O_3 preparation

First, 0.5 g of the commercial Zinc oxide was dispersed in 50 mL of the 0.2 M NaOH solution (Solution I). Second, 0.5 g of the $Bi(NO_3)_3.5H_2O$ was dissolved in 5 mL of the 1 M nitric acid solution (Solution II). Then, the solution (II) was added drop wise into the

solution (I) under constant stirring. After stirring the mixture for 30 min at 80 ºC, the product was separated by decantation, washed with double distilled water several times and dried at 60º C. Then, heat treatment of the product was carried out at 600 ºC for 1 h.

Synthesis procedure for preparing SnO$_2$

The SnO$_2$ nanoparticle was synthesized by the solid state method [12]. The SnCl$_2$. 2H$_2$O (2.2 g) and NaOH (0.8 g) were mixed in an agate mortar and were thoroughly grounded for 60 min at room temperature. The product was washed with double distilled water several times and dried at 60 °C. Then, heat treatment of the product was carried out at 900 ºC for 1 h.

Synthesis procedure for SnO$_2$/Bi$_2$O$_3$/Bi$_2$O$_4$ preparation

First, 0.5 g of the prepared tin oxide was dispersed in 50 mL of the 0.2 M NaOH solution (Solution I). Second, 0.5 g of Bi(NO$_3$)$_3$.5H$_2$O was dissolved in 5 mL of the 1M nitric acid solution (Solution II). Then, the solution (II) was added drop wise into the solution (I) under constant stirring. After stirring the mixture for 30 min at 80 ºC, the product was separated by decantation, washed with double distilled water several times and dried at 60 °C. Then, heat treatment of the product was carried out at 600 ºC for 1 h.

Evaluation of photocatalytic activity

A high pressure lamp (400W Hg) manufactured by Holland Philips, was used as the light source. Air was blown into the reaction by an aquarium pump to maintain the solution saturated with oxygen during the course of the reaction. In each experiment, 0.05 g of each prepared photocatalyst was added in 100 mL of the methylene blue solution (10 ppm). During irradiation, agitation was maintained by a magnetic stirrer to keep the suspension homogeneous. The suspension was sampled at regular intervals and immediately centrifuged to remove catalyst particles completely. Then, the degree of photo decolorization (X), as a function of time, is given by X = (C -C)/C , where, C is the initial concentration of dye, and C is the concentration of dye at time t. The progress of photocatalytic decolorization was measured by a UV-Vis spectrophotometer (Shimadzu UV-2550). The disappearance of peak at = 663 nm was chosen for monitoring of dye decolerization for a methylene blue solution (M.B.).

Results and discussion

The structure and morphology of the product were characterized by using XRD (Holland Philips Xpert, X-ray diffractometer with Cu-K radiation) and field emission scanning

electron microscope (FE-SEM) (Hitachi S-4160) with gold coating. XRD results (Figure 1a) confirmed that the α-Bi_2O_3 (monoclinic, JCPDS No. 01-071-2247) was obtained by heat treatment at 600 ℃ for 1h. XRD results (Figure 1b) revealed that the SnO_2 (tetragonal, JCPDS No. 21-1250) was obtained.
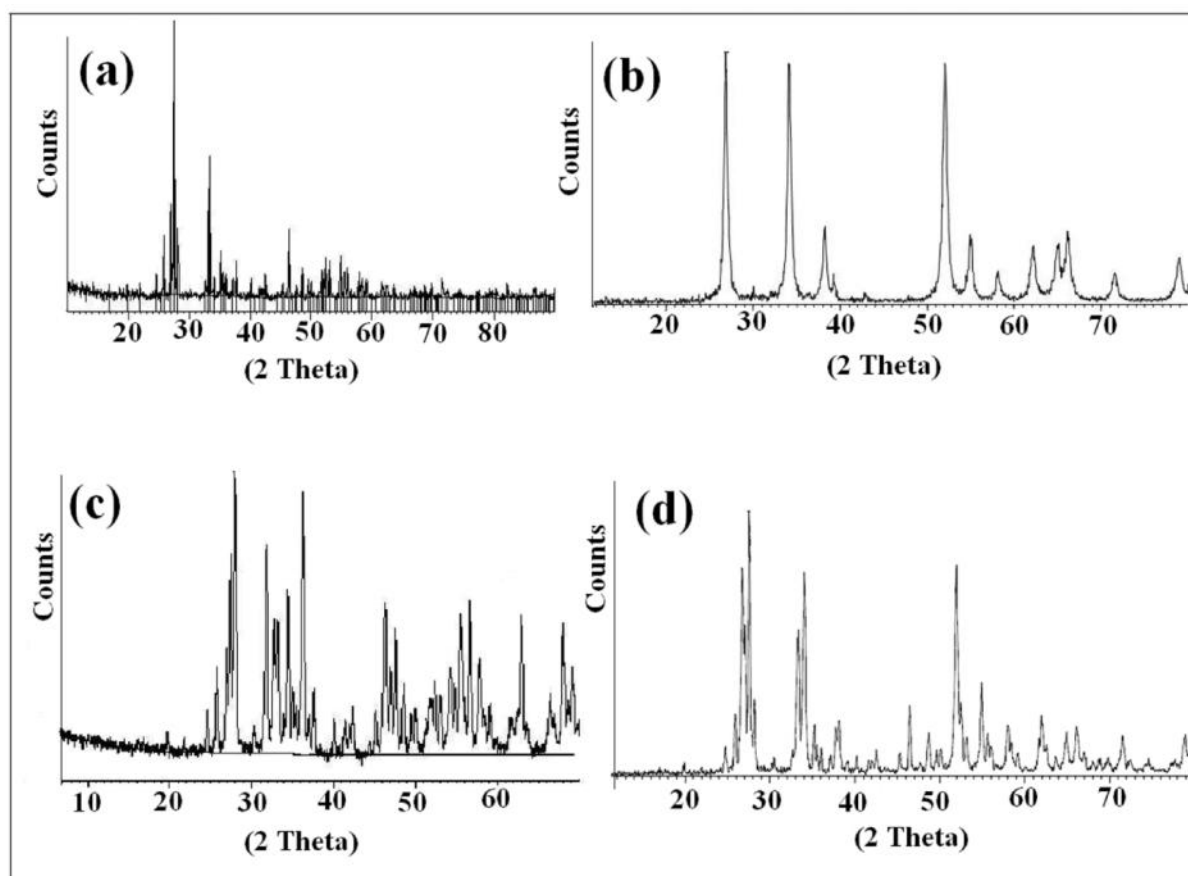
Figure 1. XRD patterns of the samples (a) α-Bi_2O_3 (b) SnO_2 (c) ZnO/Bi_2O_3 (d) $SnO_2/Bi_2O_3/Bi_2O_4$

Figure 2. FE-SEM images of the samples (a) -Bi$_2$O$_3$ (b) SnO$_2$ (c) ZnO/Bi$_2$O$_3$ (d) SnO$_2$/ Bi$_2$O$_3$/Bi$_2$O$_4$

Figure 1C shows the XRD patterns of the ZnO/Bi_2O_3 prepared after heat treatment at 600 ℃. As shown in XRD pattern monoclinic and tetragonal phase (JCPDS No. 00-029-0236, JPDS No. 01-071-2274) were observed for the Bi_2O_3. In addition, wurtzite phase was observed for the ZnO (JCPDS No. 01- 079-2205). The structure of SnO_2/Bi_2O_3/Bi_2O_4 composite was investigated by the XRD pattern (Figure 1d). As shown in the XRD pattern monoclinic phase was observed for -Bi_2O_3 (JCPDS No. 71-0465) and Bi_2O_4 (JCPDS No. 50-0864). In addition, tetragonal phase was observed for the SnO_2 (JCPDS No. 21-1250). The morphology of the samples was studied by FE-SEM (Figure 2). Figure 2a and Figure 2b show that the morphology of the Bi_2O_3 and SnO_2 samples are rod-like and nanoparticle respectively. Figure 2c illustrates that the surface of ZnO/Bi_2O_3 sample consists of nanoparticles with average size of 15.7 nm. Figure 2d indicates that the SnO_2/Bi_2O_3/Bi_2O_4 sample consists of rods with average length of 3.4 µm and nanoparticles with average size of 57.5 nm. In this work methylene blue solution was chosen as the environmental pollutant. The

results in figure 3 showed that, the dye adsorption on the surface of the prepared photocatalysts is poor after 120 min in the dark (Figures. 3a, 3b, 3c, 3d and 3e).

Figure 3f, 3g, 3h, 3i and 3j show the UV-Vis spectra changes during the light irradiation. As can be seen, Zinc oxide is a well-known photocatalyst. So far, several papers have been published on the bare zinc oxide photocatalytic activity [13-17]. In this work, the photocatalytic activity of ZnO/Bi_2O_3 sample and commercial zinc oxide have been compared. These experiments indicate whether Bi_2O_3 is improving or hampering the photocatalytic activity of ZnO/Bi_2O_3 and whether commercial zinc oxide still has the highest activity or not. The photocatalytic decolorization results show that the ZnO and ZnO/ Bi_2O_3 samples can degrade 99 and 95% of cationic M.B. dye solution after 120 min under UV-Vis irradiation respectively (Figure 4). It should be noted that the adsorption of M.B. solution on the surface of the samples is at about 8% after 120 min in the dark. According to the photocatalytic experiments, commercial zinc oxide still has the highest activity.
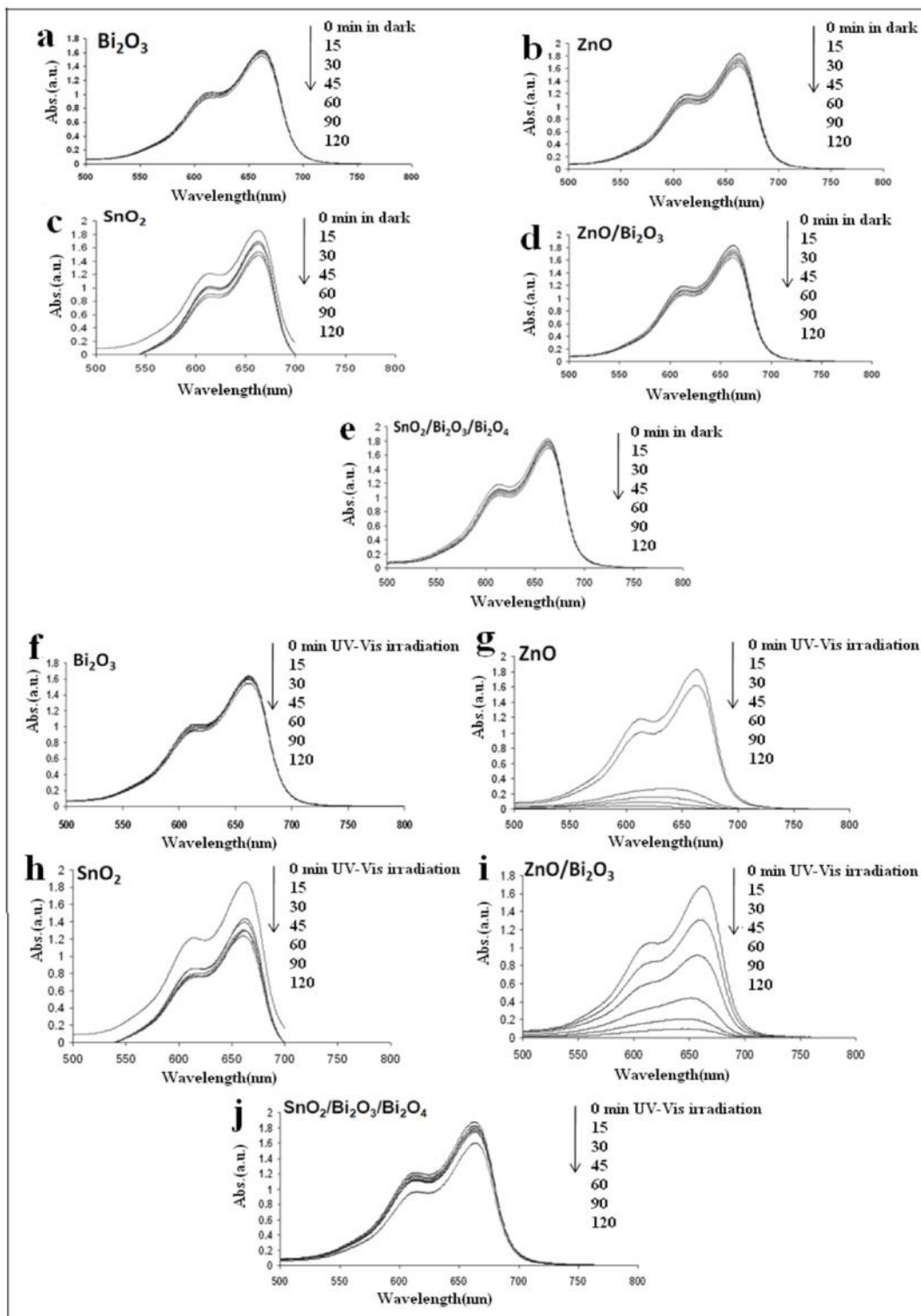
Figure 3. UV-Vis absorbance spectra of (M.B.) solution in the presence of prepared photocatalysts in dark (**a**, **b**, **c**, **d**, **e**) and light irradiation (**f**, **g**, **h**, **i**, **j**)
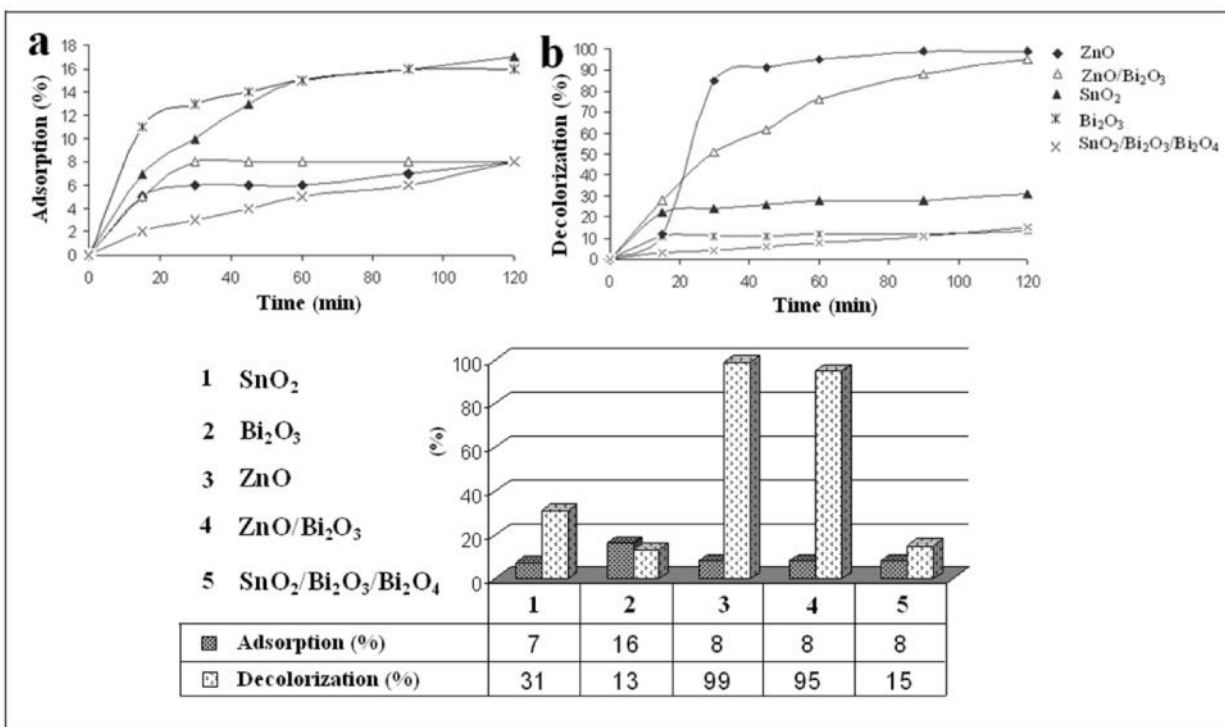
Figure 4. Adsorption and decolorization percentage of (M.B.) solution in the presence of prepared photocatalysts

To have a quantitative estimate of the photocatalytic activity of the prepared samples the optical band gap *via* the Tauc Equation was employed ($h v = A(h v - E_g)$). In this equation   is the absorption coefficient, *hv* is the photon energy, E_g is the optical band gap, *A* which is a constant does not depend on the photon energy and   has four numeric values ($\frac{1}{2}$ for allowed direct transitions, 2 for the allowed indirect, 3 for forbidden direct and $\frac{3}{2}$ for forbidden indirect optical transitions) [18, 19]. In this work, the direct transition band gap (E_g) of the samples was determined by plotting ($h v)^2$ versus *h*

curve with the extrapolation of the linear region to ($h v)^2 = 0$ [20, 21]. Figure 5 (**a-c**) illustrates the ($h v)^2$ vs. *hv* for Bi_2O_3, ZnO and ZnO/Bi_2O_3 samples. The values of band gap for Bi_2O_3 and ZnO are found to be 2.8 eV. and 3.4 eV. respectively. Figure 5d presents UV-Vis spectra of the Bi_2O_3, ZnO and ZnO/Bi_2O_3 samples. As shown the commercial zinc oxide, Bi_2O_3, and ZnO/Bi_2O_3 have a broad peak at about 361-460 nm. The Figures 6a and 6b show the ($h v)^2$ vs. *hv* for SnO_2 and $SnO_2/Bi_2O_3/Bi_2O_4$ samples. The value of band gap for SnO_2 and $SnO_2/Bi_2O_3/Bi_2O_4$ is found to be 2.8 eV. Figure 6c illustrates UV-Vis spectra of the

Bi$_2$O$_3$, SnO$_2$ and SnO$_2$/Bi$_2$O$_3$/Bi$_2$O$_4$ samples. According to Figure 5c, for ZnO/Bi$_2$O$_3$ composite two band gap values (2.8 eV. and 3.4 eV.) are observed. These values are related to bare Bi$_2$O$_3$ and ZnO respectively. Figure 6b shows that the band gap value of the SnO$_2$/Bi$_2$O$_3$/Bi$_2$O$_4$ composite is 2.8 eV.
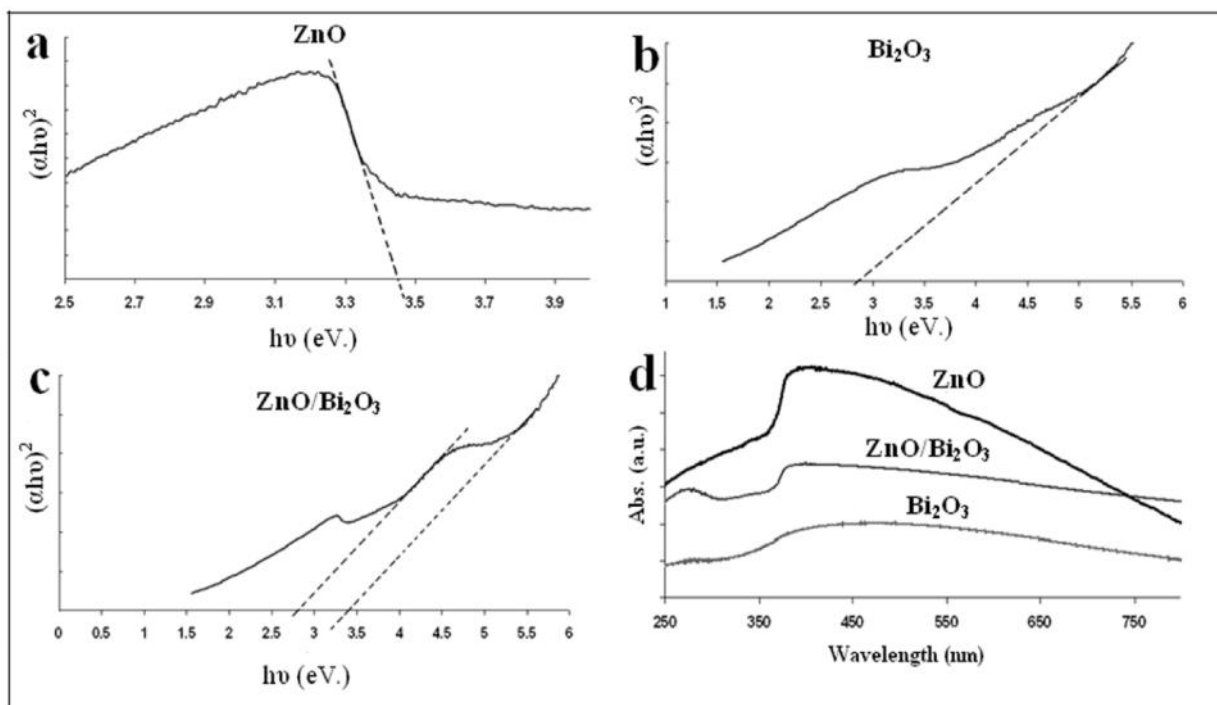
Figure 5. The plot of $(\alpha h\upsilon)^2$ versus $h\upsilon$, (a) ZnO, (b) Bi$_2$O$_3$, (c) ZnO/Bi$_2$O$_3$ composite, (d) UV-Vis absorbance spectra of the ZnO, Bi$_2$O$_3$ and ZnO/Bi$_2$O$_3$ samples

The photoluminescence spectrum (PL) of commercial zinc oxide is shown in Figure 7. The emission bonds show a strong and broad UV-blue emission at about (393-440 nm) and a weak green emission at about 508 nm. UV emission is due to the recombination of the generated electrons and holes, related to the near-band edge emission. Luminescence spectroscopy is known to be an effective method for evaluation of surface defects and optical properties. Generally, the blue and blue-green emissions are possibly due to the surface defects and the green emission corresponds to the singly ionized oxygen vacancy in the zinc oxide [21-23].
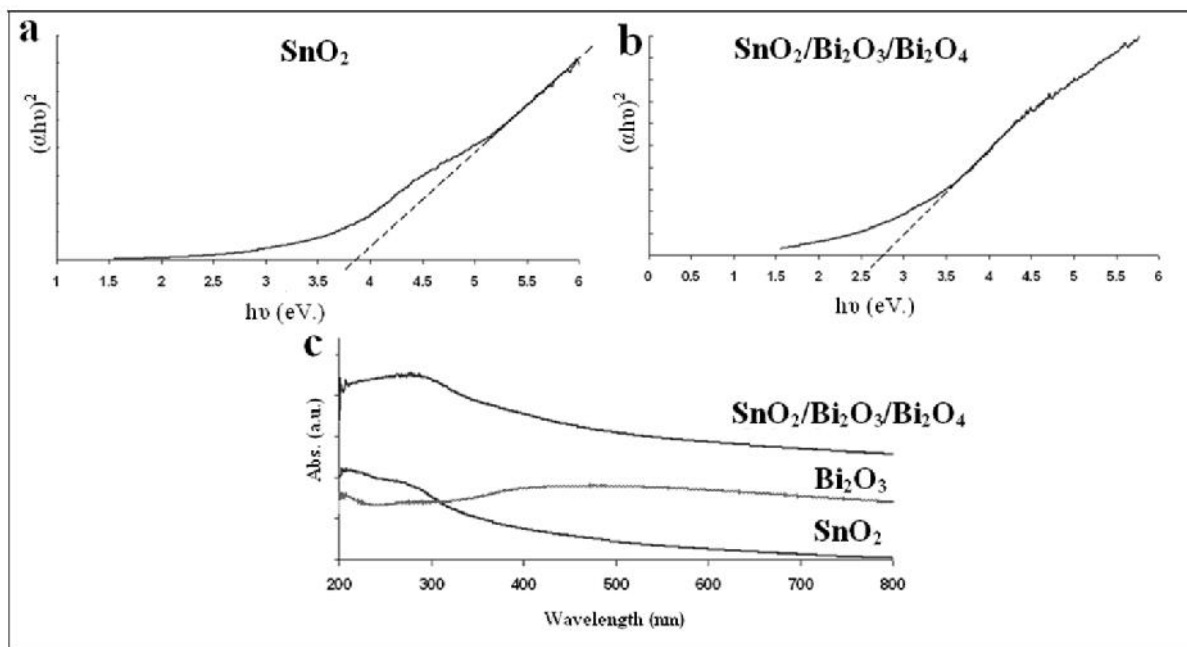
Figure 6. The plot of $(\alpha h\nu)^2$ versus $h\nu$, (a) SnO_2, (b) $SnO_2/Bi_2O_3/Bi_2O_4$ composite, (c) UV-Vis absorbance spectra of the SnO_2, Bi_2O_3 and $SnO_2/Bi_2O_3/Bi_2O_4$ samples
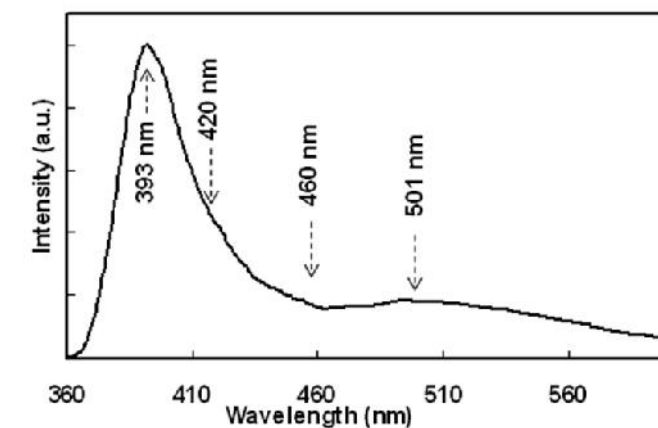
Figure 7. The PL spectrum of commercial zinc oxide

Deep level emission is related to various defects such as zinc interstitials (Zn_i), oxygen vacancies (V_O), Zn vacancies (V_{Zn}), and antisite-defect oxygen substitution zinc (O_{Zn}) [24, 25]. The interstitial Zn (Zn_i), ($\sim$ 0.4-0.5 eV.) is located at the bottom of the conduction band. Hence, interstitial Zn (Zn_i) acts as an electron acceptor [26, 27]. The interstitial Zn (Zn_i) defect inhibits recombination of photogenerated hole (h^+)

and electron (e$^-$), therefore, commercial zinc

oxide has the highest photocatalytic activity.
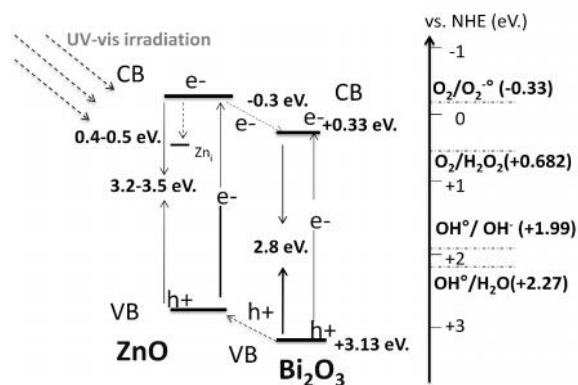
Figure 8. Schematic diagram of photoexited electrons-holes separation process for the ZnO/Bi$_2$O$_3$ system
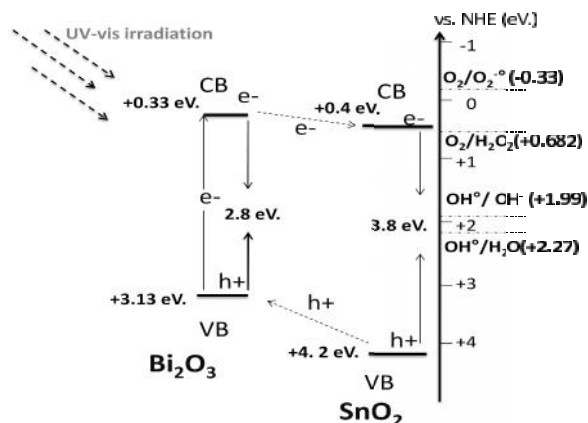
Figure 9. Schematic diagram of photoexited electrons-holes separation process for the SnO$_2$/Bi$_2$O$_3$ system

Figure 8 and Figure 9 show the mechanism of the charge separation and photocatalytic reaction for the ZnO/Bi$_2$O$_3$ and SnO$_2$/Bi$_2$O$_3$ semiconductors. As illustrated in the scheme, when the composites are irradiated by the UV light with the photon energy higher than that of the ZnO and SnO$_2$ band gaps, electrons in the valence band (VB) are excited to the conduction band (CB) with the simultaneous generation of the same amount of holes (h$^+$) in the VB. The Bi$_2$O$_3$ has a relatively narrow band gap (2.8 eV.). As the position of conduction band of -Bi$_2$O$_3$ (E$_{CB}$=+0.33 eV., E$_{VB}$=+3.13 eV.) is lower than that of ZnO (E$_{CB}$=-0.3 eV., E$_{VB}$=+2.9 eV.) [26, 27] it can act as a photoelectronic receiver as represented in Figure 8.

The valence band position of the ZnO is more positive than the standard redox potential of ($^\bullet$OH/OH$^-$ =1.99 eV., vs. NHE) [28], suggest that the generated holes in the valence band of ZnO can oxidize OH$^-$ or H$_2$O to form $^\bullet$OH, which is then involved in the photocatalytic degradation of M.B. solution. The conduction band edge potential of -Bi$_2$O$_3$ (+0.33 eV.) which is more positive than the standard redox potential (O$_2$/$^\bullet$O$_2^-$ =-0.33 eV., vs. NHE) and (O$_2$/$^\bullet$HO$_2$=-0.046 eV., vs. NHE) [29, 30], suggest that the electrons in the conduction band of -Bi$_2$O$_3$ cannot reduce O$_2$ to $^\bullet$O$_2^-$ and $^\bullet$HO$_2$. However, the accumulated electrons in the conduction band of -Bi$_2$O$_3$ can be transferred to O$_2$ adsorbed on the surface of the composite semiconductors and H$_2$O$_2$ yields because the conduction band level of -Bi$_2$O$_3$ is more

negative than the standard redox potential $(O_2/H_2O_2=+0.682$ eV., vs. NHE) [31]. The above processes initiate photocatalytic oxidation reactions. As the position of the conduction band of SnO_2 ($E_{CB}=+0.$ 4 EV., $E_{VB}=+4.$ 2 eV.) is slightly lower than that of -Bi_2O_3 ($E_{CB}=+0.33$ eV., $E_{VB}=+3.13$ eV.) [25], it can acts as a photoelectronic receiver as represented in Figure 9. Conversely, the holes transfer from the VB of SnO_2 to that of Bi_2O_3. The photogenerated electrons and holes in the composite could be injected into a reaction medium and participate in chemical reactions. The SnO_2/Bi_2O_3 system inhibited the recombination of photogenerated hole (h^+) and electron (e^-) in Bi_2O_3. But results show that the photoactivity of the SnO_2/Bi_2O_3 system was not improved. To sum up, position of energy levels and separation of photogenerated electron/hole pairs are important for the efficient photocatalytic performance. In present study the reusability of ZnO/Bi_2O_3 has also been investigated. At the end of each cycle the ZnO/Bi_2O_3 catalyst was washed with double distilled water and a fresh solution of methylene blue was added before each photocatalytic run. The decolorization rates for the five cycling reuse were 100, 98, 95 and 90 % after 120 min of reaction time (Figure 10).
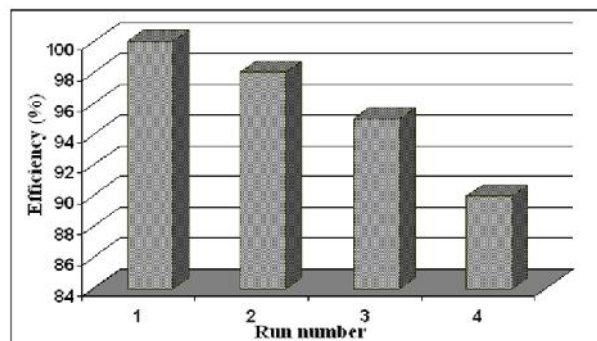
Figure 10. Reusability of the ZnO/Bi_2O_3 composite

Conclusion

In conclusion, the $SnO_2/Bi_2O_3/Bi_2O_4$, ZnO/Bi_2O_3 nanocomposites, Bi_2O_3 rods and SnO_2 nanoparticle have been synthesized using the simple route. The present work shows that the photocatalytic performance of the ZnO/Bi_2O_3 is higher than that of Bi_2O_3, SnO_2 and $SnO_2/Bi_2O_3/Bi_2O_4$ which is related to the presence of zinc oxide. The enhancement of the photocatalytic activity is attributed to the energy level position and separation of photogenerated electron/hole pairs.

References

[1] L. Han, X. Zhou, L. Wan, Y. Deng, S. Zhan, *J. Environ. Chem. Engin.*, **2014**, *2*, 123-130.

[2] K. Dia, L. Lu, C. Liang, J. Dia, G. Zhu, Z. Liu, Q. Liu, Y. Zhang, *Mater. Chem. Phys.*, **2014**, *143*, 1410-1416.

[3] T. Ghosh, K.y. Cho, K. Ullah, V. Nikam, C.Y. Park, Z.D. Meng, W.C. Oh, *J. Industrial and Engin. Chem.*, **2013**, *19*, 797-805.

[4] R.M. Mohamed, E.S. Baeissa, *J. Industrial and Engin. Chem.*, **2014**, *20*, 1367-1372.

[5] A.R. Mahjoub, M. Movahedi, E. Kowsari, I. Yavari, *Mater. Sci. Semicond. Processing*, **2014**, *22*, 1-6.

[6] T. Okuno, G. Kawamura, H. Muto, A. Matsuda, *J. Mater. Sci. & Tech.*, **2014**, *30*, 8-12.

[7] J.S. Lee, J. Jang, *J. Industrial and Engin. Chem.*, **2014**, *20*, 363-371.

[8] S. Kumar, B. Kumar, T. Surendar, V. Shanker, *Mater. Research. Bull.*, **2014**, *49*, 310-318.

[9] H.H. Chun, W.K. Jo, *J. Industrial and Engin. Chem.*, **2014**, *20*, 1010-1015.

[10] Q. Wang, H. Jiang, S. Zang, J. Li, Q. Wang, *J. Alloys and Compds*, **2014**, *586*, 411-419.

[11] Y. Wang, J. Zhao, Z. Wang, *Colloids Surf. A: Physicochem. Eng. Aspects*, **2011**, *377*, 409-413.

[12] A.A. Firooz, A.R. Mahjoub, A.A. Khodadadi, *Mater. Chem. Phys.*, **2009**, *115*, 196-199.

[13] J.C. Sin, S.M. Lam, K.T. Lee, A.R. Mohamed, *Mater. Sci. Semicond. Processing*, **2013**, *16*, 1542-1550.

[14] U.I. Gaya, A.H. Abdullah, M.Z. Hussein, Z. Zainal, *Desalination*, **2010**, *263*, 176-182.

[15] B. Zhao, C.L. Wang, Y.W. Chen, H.L. Chen, *Mater. Chem. Phys.*, **2010**, *121*, 1-5.

[16] J.B. Zhong, J.Z. Li, Z.H. Xiao, W. Hu, X.B. Zhou, X.W. Zheng, *Mater. Lett.*, **2013**, *91*, 301-303.

[17] X. Zhao, M. Li, X. Lou, *Mater. Sci. Semicond. Processing*, **2013**, *16*, 489-494.

[18] J. Tauc, R. Grigorovici, A. Vancu, *Phys. Status. Solidi*, **1966**, *15*, 627–637.

[19] S.J. Pearton, D.J. Norton, K. Ip, Y.W. Heo, T. Steiner, *Prog. Mater. Sci.* **2005**, *50*, 293-340.

[20] S.C. Lyu, Y. Zhang, H. Ruh, H.J. Lee, H.W. Shim, E.K. Suh, C.J. Lee, *Chem. Phys. Lett.* **2002**, *363*, 134–138

[21] S. Monticone, R. Tufeu, A.V. Kanaev, *J. Phys. Chem. B.*, **1988**, *102*, 2854-2862.

[22] O.D. Jayakumar, V. Sudarsan, C. Sudakar, R. Naik, R.K. Vatsa, A.K. Tyagi, *Scripta Materialia*, **2010**, *62*, 662-665.

[23] S. Singh, M.S. Ramachandra, *Scripta Materialia*., **2009**, *61*, 169-172.

[24] K. Vanheusden, W.L. Warren, C.H. Seager, D.R. Tallant, J.A. Voigt, B.E. Gnade, *J. Appl. Phys*., **1996**, *79*, 7983-7990.

[25] B. Lin, Z. Fu, Y. Jia, *Appl. Phys. Lett*., **2001**, *79*, 943-945.

[26] A.M. Abdulkarem, A.A. Aref, A. Abdulhabeeb, Y.F. Li, Y. Yu, *J. Alloys and Compds*, **2013**, *560*, 132-141.

[27] B. Subash, B. Krishnakumar, M. Swaminathan, M. Shanthi, *Powder Tech*., **2013**, *241*, 49-59.

[28] X. L. Fu, W.M. Tang, L. Ji, S.F. *Chen, Chem. Eng. J*., **2012**, *180*, 170-177.

[29] Z.H. Li, Z.P. Xie, Y.F. Zhang, L. Wu, X.X. Wang, X.Z. Fu, *J. Phys. Chem. C*., **2007**, *111*, 18348-18352.

[30] S. Anandan, M. Miyauchi, *Chem. Commun*., **2012**, *48*, 4323-4325.

[31] M. Antoniadou, P. Lianos, *Appl. Catal. B: Environ*., **2010**, *99*, 307-313.